*European Cells and Materials* Vol.48 2024 (pages 156–167) DOI: 10.22203/eCM.v048a10 ISSN 1473-2262

*Original Article*

# PROPOFOL NANOPARTICLES PROMOTE FRACTURE HEALING IN MICE BY ACCELERATING CARTILAGE FORMATION

B.Y. Zhang[1,§], Z. Wang[1,§], S.J. Yan[2] and H. Wang[3,*]

[1]Department of Anesthesiology, The Second Affiliated Hospital of Shandong First Medical University, 271000 Tai'an, Shandong, China
[2]Pharmacy Department, Tai'an Central Hospital (Tai'an Central Hospital affiliated to Qingdao University, Mount Taishan Medical Center), 271000 Tai'an, Shandong, China
[3]Department of Orthopedics, Yantaishan Hospital, 264000 Yantai, Shandong, China
[§]These authors contributed equally.

**Abstract**

**Background**: Fracture healing is a process characterized by cartilage formation and subsequent ossification. Propofol, a systemic anesthetic known for its anti-inflammatory and chondrogenic properties, was encapsulated into nanoparticles (NPs) to improve its therapeutic efficacy. This study investigates the impact of these nanoparticles on fracture healing in a murine model. **Methods**: Propofol-NPs were synthesized and administered in a mouse femoral fracture model. Post-fracture, mice were randomly allocated to control, propofol, or propofol-NPs groups, with the latter receiving daily intraperitoneal injections. Fracture healing was evaluated through Hematoxylin and Eosin (HE) and Masson's trichrome staining, along with motor function assessments. *In vitro*, bone marrow-derived mesenchymal stem cells (BMSCs) were induced to differentiate into chondrocytes, and propofol's effects on differentiation were analyzed. Additionally, cell migration was assessed via scratch and Transwell assays. Western blot analysis was performed to quantify the expression of bone morphogenetic protein (BMP)2, aggrecan, Collagen Type II Alpha 1 Chain (Col2a1), activin receptor-like kinases (Alk)2, osterix (OSX), $\beta$-catenin, and collagen I (COL1) in differentiated BMSCs. **Results**: Propofol treatment significantly accelerated fracture healing and improved bone quality compared to the control group ($p < 0.01$). The propofol-NPs group exhibited a marked enhancement over the propofol group ($p < 0.05$). Both treatments facilitated BMSC differentiation into chondrocytes and upregulated key differentiation markers ($p < 0.01$). BMP2, aggrecan, Col2a1, activin receptor-like kinases (Alk)2, and phosphorylated $\beta$-catenin (p-$\beta$-catenin) levels were significantly increased after propofol and propofol-NPs treatment ($p < 0.01$), with OSX and COL1 also upregulated. Propofol-NPs demonstrated superior therapeutic efficacy over propofol alone. **Conclusions**: Propofol-NPs enhance fracture healing in mice by promoting cartilage formation and BMSC differentiation, offering promising potential for clinical applications in fracture repair.

**Keywords:** Propofol nanoparticles, fracture healing, cartilage formation, BMSCs, chondrogenesis.

***Address for correspondence**: H. Wang, Department of Orthopedics, Yantaishan Hospital, 264000 Yantai, Shandong, China. Email: zfythai@163.com.



## Introduction

Fracture healing is a multifaceted biological process that involves the intricate regulation of various cell types and signaling pathways (Schlickewei *et al*., 2019; Bahney *et al*., 2019). Among the pivotal stages, cartilage formation significantly impacts both the rate and quality of healing (Clark *et al*., 2020). Cartilage serves as a structural scaffold essential for bone tissue regeneration (Bahney *et al*., 2019; Saul and Khosla, 2022), making the exploration of its regulatory mechanisms critical for a deeper understanding of fracture repair (Ghiasi *et al*., 2019).

The formation of chondrocytes and subsequent matrix calcification are key events in this process (Kodama *et al*., 2022; Cheng *et al*., 2020). Cartilage functions as a provisional scaffold, providing a necessary substrate for new bone tissue formation (Liu *et al*., 2020b; Zhang *et al*., 2019). The formation of chondrocytes and the subsequent calcification of the cartilage matrix are essential stages in cartilage formation, regulated by several key signaling pathways, including bone morphogenetic protein (BMP), wingless-related integration site (Wnt), and fibroblast growth factor (FGF) pathways, along with molecular regulations (Sivaraj *et al*., 2022). Chondrocyte development occurs through the differentiation of precursor cells, such as mesenchymal stem cells, into chondrocytes, mediated by these signaling pathways and regulatory factors like BMP, Wnt, and FGF (Chilbule *et al*., 2021; Kim *et*

*al*., 2021). These pathways activate specific transcription factors, which regulate gene expression and drive the differentiation of stem cells into chondrocytes, leading to the formation of cartilage tissue (Zhang *et al*., 2022).

Cartilage matrix calcification, integral to the cartilage-to-bone transition, entails the deposition of calcium ions and phosphate into the cartilage matrix, forming a calcified matrix. This phase is governed by molecular regulators such as alkaline phosphatase (ALP), phosphoproteins, osteopontin, osteocalcin, and collagen (Zhu *et al*., 2020; Deng *et al*., 2020). Proteins like BMP2, aggrecan, Collagen Type II Alpha 1 Chain (Col2a1), and activin receptor-like kinases (Alk)2 are crucial in driving chondrocyte differentiation and participate in the mineralization and calcification of the matrix, thus facilitating the conversion of cartilage into bone.

Propofol, a commonly used anesthetic in clinical settings, is known for its sedative, analgesic, and muscle relaxant effects (Xu *et al*., 2020; Peng *et al*., 2020). When formulated into nanoparticles (NPs), propofol's stability is significantly improved (Luo *et al*., 2020). Recent research has indicated that propofol may positively influence fracture healing, offering promising potential for therapeutic applications in this field (Lee *et al*., 2018). However, the specific mechanisms through which propofol enhances cartilage formation during fracture repair remain unclear. Given the critical role of cartilage in the fracture healing process, a thorough investigation into propofol's effects is of notable clinical importance.

This study aims to evaluate the influence of propofol on cartilage formation during fracture healing and to elucidate its underlying mechanisms. A murine femoral fracture model was employed to assess propofol's impact on cartilage formation. Additionally, *in vitro* experiments were conducted to explore how propofol affects the differentiation of bone marrow-derived mesenchymal stem cells (BMSCs) into chondrocytes. These investigations aim to provide a comprehensive understanding of propofol's mechanism of action in cartilage formation during fracture healing, laying a stronger theoretical foundation for its clinical application in enhancing fracture repair.

## Methods

*Propofol Nanoparticle Preparation*

An appropriate carrier material, polyvinylpyrrolidone (PVP, P8290, Solarbio, Beijing, China), was selected, based on the methods of Zhang *et al*. (2015) and Chen *et al*. (2021) with slight modifications. Propofol (5 mg, YZ-100806, Solarbio, Beijing, China) and PVP (20 mg) were added to methanol (10 mL, 10014108, HUSHI, Shanghai, China) and stirred overnight. The nanoparticles were characterized by particle size distribution, zeta potential, and morphology. Dynamic light scattering (DLS) was used for analysis of the propofol nanoparticles using a Malvern Zetasizer Nano ZS (zs90, Malvern Instrument, Great Malvern, UK) with a 3 mW He/Ne laser at 633 nm. After lyophilization, the propofol nanoparticles were rehydrated with 0.1 mg/mL distilled water for analysis. The release of propofol was measured through UV/visible absorption at 285 nm, corresponding to a pH of 7.4, which represents blood pH.

*Encapsulation Efficiency (EE) Determination*

Nano-carrier samples containing the drug were prepared, and the separation of unencapsulated free drug from the encapsulated drug in the carrier was carried out using methods such as ultrafiltration, gel filtration, or gel electrophoresis. The concentration of the free drug was quantified by spectrophotometry. EE was calculated using the formula: EE = (Total amount of drug – Amount of free drug)/Total amount of drug × 100 %. Additionally, drug loading (DL) was determined by the following formula: DL = (Drug Mass/Total Carrier Mass) × 100 %.

*Electron Microscopy Scanning*

The lyophilized propofol nanoparticles were rehydrated with 0.1 mg/mL distilled water and centrifuged at 2500 g. The samples were then examined under an electron microscope (quanta 200; Thermo Fisher Scientific, Waltham, MA, USA). Appropriate electron microscope parameters were set, and the sample was scanned to obtain images, which were analyzed for particle shape, size distribution, and microstructural morphology.

*Mouse Fracture Model*

Twelve male C57/BL6J mice (aged 8–10 weeks, body weight 30 ± 2 g) were obtained from the Chinese Academy of Sciences Laboratory Animal Resources Platform. The mice were anesthetized with an intraperitoneal injection of 20 g/L pentobarbital sodium (30 mg/kg, 21642-83-1, Shandong Xiya Chemical Industry Co., Ltd., Linyi, China) and subjected to a standard mouse unstable tibial fracture model. The detailed procedure was as follows: the fur on the left lower limb knee joint was removed, the area was disinfected, and a longitudinal incision was made in the skin to expose and detach the knee ligament. A hole was drilled between the tibial condyles, and a sterile Kirschner wire (KSH0840F, PurrWoof, Changzhou, China) with a diameter of 0.1 mm was inserted into the medullary cavity. The muscle at the midshaft of the tibia was bluntly dissected, and a transverse fracture of the tibia was induced. The incision was then closed in layers following sterile phosphate-buffered saline (PBS) irrigation. The experimental group received daily injections of propofol solution (1261393-54-7, Merck, Darmstadt, Germany) at 10 mg/kg into the muscles surrounding the fracture site, based on Chen *et al*. (2021), while the control group was injected with 0.3 mL of saline (BL158A, Biosharp Life Science, Hefei, China). In the propofol-nanoparticles (NPs) group, mice received daily injections of 10 mg/kg propofol nanoparticles, following Zhou *et al*. (2021). The mice were housed in individual

cages under controlled temperature conditions (22–24 °C), provided with standard feed, free access to water, and allowed free movement. Seven days after the fracture model was established, the mice were euthanized via intraperitoneal injection of pentobarbital sodium (100 mg/kg), and tissue samples were collected.

*Behavioral Testing*

To assess post-fracture recovery in mice, both a lattice walking test and a rotating rod test were conducted. The rotating rod apparatus consists of a barrel with a diameter of 3 cm, divided into four runways by a 10 cm high wall. Mice underwent training on the first day, followed by testing on the second day. During the test, the rotational speed accelerated from 0.0027 g to 0.27 g, with an increment of 0.00017 g every 8 seconds, and the duration that the mice remained on the rod (up to 5 minutes) was recorded. The grid walking test evaluated motor recovery by assessing the ability of the mice to move on a grid with dimensions of 2.5 × 3 × 2.5 cm. Initially, mice were required to walk in an open space for over 30 seconds. Subsequently, when tested on the grid, any instance where a hind leg completely slipped through the grid and all toes extended past the grid surface was marked as an error. The time taken by each mouse to traverse the grid was measured.

*HE Staining*

Femoral tissue from the central lesion area was collected and fixed in 4 % paraformaldehyde (P1110, Solarbio, Beijing, China) for 24 hours, followed by decalcification using 15 % ethylenediaminetetraacetic acid (EDTA, T1300, Solarbio, Beijing, China) for 3 weeks, with the solution being replaced every 3 days. The samples were then embedded in paraffin and sectioned into 5 $\mu$m slices using a microtome. Hematoxylin and Eosin (HE) were obtained from Solarbio (G1120, Beijing, China). Slices were dewaxed and hydrated for 5 minutes, stained with hematoxylin for 5 minutes, and subsequently with 0.5 % eosin for 10–15 seconds. After washing with distilled water, dehydration was carried out using ethanol, followed by slide sealing and microscopic observation (CX53, Olympus, Tokyo, Japan). Quantitative image analysis was performed using ImageJ software (version 1.5f, National Institutes of Health, Bethesda, MD, USA).

*Masson Staining*

Tissue samples were also assessed using Masson's Trichrome Stain Kit (G1340, Solarbio, Beijing, China). Sections were stained with Weigert's iron hematoxylin for 5 minutes, followed by treatment with phosphomolybdenum-phosphotungstic acid for 45 seconds. After 5 minutes of staining with a solution containing 1 % orange G and 0.25 % aniline blue, the slides were washed with 1 % acetic acid solution and stained for 20 minutes with 0.12 % ponceau xylidine. The slides were then dried with ethanol and xylene, rinsed with 1 % acetic acid solution, and incubated with 2.5 % phosphotungstic acid for 10 minutes.

*Culture of BMSCs*

One mouse was randomly selected, euthanized, and immersed in 75 % ethanol for 12 minutes for disinfection. Under sterile conditions, the femur and both tibiae were collected, and bone marrow-derived mesenchymal stem cells (BMSCs) were isolated by removing the bone ends. The cells were cultured and passaged at a 1:2 ratio, with cell growth being monitored. The cells were passaged at a 1:3 ratio once they reached 80 %–90 % confluence. After five passages and further expansion, the BMSCs were cultured until 80 % confluence was reached. The medium was then replaced, and 20 mmol/L BrdU (ab6326, Abcam, Cambridge, MA, USA) was added for cell labeling. The surface marker CD73 (ab288154, Abcam, Cambridge, MA, USA) was identified using flow cytometry (CytoFLEX, Beckman Coulter, Inc., Brea, CA, USA), and the cells were tested for mycoplasma contamination.

*BMSC Identification Experiment and Flow Cytometry*

The morphological characteristics of BMSCs, including shape, size, and adherence to the substrate, were observed using a microscope (CX31; Olympus, Tokyo, Japan). Special attention was given to the morphological heterogeneity of the cells, which is a hallmark of MSCs. Flow cytometry analysis was conducted using APC-conjugated anti-mouse CD73 and FITC-conjugated anti-mouse CD90 (ab155378, ab11155, Abcam, Cambridge, MA, USA) to identify MSC surface markers, utilizing the BD FACSCanto system (BD FACSCanto; BD Biosciences, Franklin Lakes, NJ, USA).

*BMSC Differentiation and Staining*

For lineage-specific differentiation, two types of experiments were performed: osteogenesis and chondrogenesis. Cells were seeded at a density of 1 × $10^5$ cells per well in appropriate media (Cyagen Biosciences, Guangzhou, China). The osteogenic differentiation medium (MUBMX-90021) contained 10 % fetal bovine serum (FBS), 0.1 $\mu$m dexamethasone, 0.2 mM ascorbic acid, and 10 mM $\beta$-glycerophosphate, with medium changes every three days. The chondrogenic differentiation medium (MUBMX-9004) consisted of 10 % FBS, 10 ng/mL transforming growth factor-$\beta$1 (TGF-$\beta$1), 0.1 $\mu$m dexamethasone, 50 $\mu$g/mL ascorbic acid, and 6.25 $\mu$g/mL transferrin, also refreshed every three days. Different drugs were administered every two days at a concentration of 5 $\mu$g/mL. After 14 days of culture, alizarin red staining was used to assess osteogenic differentiation, while alcian blue staining was applied to evaluate chondrogenic formation.

*Cell Counting Kit-8 (CCK-8) Assay*

The proliferation capacity of BMSCs was measured using the CCK-8 kit (C0037, Biotechnology, Shanghai, China). In a 96-well plate, cells were planted at a density of $3 \times 10^3$ per well. After adding 10 $\mu$L of CCK-8 solution and 100 $\mu$L of new medium to each well, the mixture was incubated for 30 minutes at 37 °C. Absorbance was read at 450 nm using a microplate reader (iMark, Bio-RAD, Hercules, CA, USA).

*Cell Scratch Assay*

For the scratch assay, cells were cultured in a 12-well plate at a density of approximately $1 \times 10^3$ cells per well. Once confluence was achieved, a cell-free area was created with a 200 $\mu$L pipette tip. Group A received 50 $\mu$L of PBS per well, and Group B received 50 $\mu$L of propofol solution. Scratch closure was evaluated 48 hours after treatment, and the experiment was repeated three times. Quantitative analysis was conducted using ImageJ software (version 1.5f, National Institutes of Health, Bethesda, MD, USA).

*Transwell Migration and Invasion Assay*

For the Transwell migration assay, cells were adjusted to a concentration of $4 \times 10^5$/mL in DMEM/F12 (D6501, Solarbio, Beijing, China) without FBS. A 100 $\mu$L cell suspension was added to the upper chamber of the Transwell (G4740, Solarbio, Beijing, China), and after 20 hours of incubation, non-migrated cells were removed from the inner side of the upper chamber by washing with PBS. The chamber was then fixed with 4 % paraformaldehyde for 15 minutes and stained with 0.1 % crystal violet for 15 minutes. Following air drying, cell migration was observed under a microscope (DM5000, Leica Microsystems, Wetzlar, Germany), and cell counts were performed manually. For the invasion assay, 60 $\mu$L of Matrigel (diluted 1:8) was precoated in the Transwell chamber to assess the cells' invasive capabilities. Quantitative analysis was carried out using ImageJ software (version 1.5f, National Institutes of Health, Bethesda, MD, USA).

*Western Blot Analysis*

Cells cultured for 2 weeks were lysed using RIPA buffer (R0010, Solarbio, Beijing, China), and protein quantification was carried out using the BCA method. Following this, electrophoresis and membrane transfer were performed. The membrane was blocked with 5 % non-fat milk at 37 °C for 2 hours. The following primary antibodies were applied: BMP2 (1:1000, ab284387, Abcam, Cambridge, MA, USA), aggrecan (1:1000, ab313636, Abcam, Cambridge, MA, USA), Col2a1 (1:1000, H00001280-M06, Thermo Fisher Scientific, Wilmington, MA, USA), Alk2 (1:1000, X1482P, Thermo Fisher Scientific, Wilmington, MA, USA), phosphorylated $\beta$-catenin (p-$\beta$-catenin) (1:1000, AP0524, ABClonal, Wuhan, China), $\beta$-catenin (1:1000, A11932, ABClonal, Wuhan, China), glyceraldehyde-3-phosphate dehydrogenase (GAPDH) (1:1000, ab8245, Abcam, Cambridge, MA, USA), osterix (OSX) (1:1000, ab209484, Abcam, Cambridge, MA, USA), and collagen I (COL1) (1:1000, ab270993, Abcam, Cambridge, MA, USA). Membranes were incubated with the primary antibodies overnight at 4 °C. After washing, horseradish peroxidase (HRP)-conjugated goat anti-rabbit secondary antibodies (1:2000 dilution, Cat # ZB-2305, ZSGB-BIO, Beijing, China) and HRP-conjugated goat anti-mouse secondary antibodies (1:2000 dilution, Cat # ZB-2301, ZSGB-BIO, Beijing, China) were applied, followed by incubation at 37 °C for 2 hours. After additional washing, enhanced chemiluminescence (ECL) chemiluminescent substrate was applied, and the membrane was exposed using a gel imaging system (Gel Doc™ EZ System; Bio-Rad Laboratories, Hercules, CA, USA). Band intensity was quantified using ImageJ software (version 1.5f, National Institutes of Health, Bethesda, MD, USA).

*Statistical Analysis*

Statistical analyses were performed using SPSS 22.0 software (International Business Machines Corporation, Armonk, NY, USA). Quantitative data are presented as mean ± standard deviation (SD). An unpaired *t*-test was used to compare differences between two groups, while multiple comparisons were analyzed using one-way or two-way ANOVA. A $p$-value $< 0.05$ was considered statistically significant.

## Results

*Propofol-NPs Physicochemical Property Characterization and BMSCs Identification*

As shown in Table 1 and Fig. 1, propofol-loaded nanoparticles (propofol-NPs) exhibited a particle size of 126.33 ± 4.59 nm, an encapsulation efficiency of 65.02 % ± 0.54, a drug payload of 32.24 % ± 0.39, a polydispersity index of 0.11 ± 0.01, and a negative surface charge of –17.23 ± 0.05 mV. The particle size distribution chart and electron microscopy images of the propofol-NPs are presented in Fig. 1**a,b**. Fig. 1**c** demonstrates that the hydrodynamic radius of the nanoparticles remained stable for the first 50 minutes before increasing sharply, suggesting that the structural integrity of the nanoparticles is most stable within this time frame. Spindle-shaped BMSCs were observed under an inverted microscope, confirming their morphology, as shown in Fig. 1**d**. Flow cytometry analysis revealed that CD73 (94.7 %) and CD90 (95.8 %) were highly expressed in the isolated BMSCs, as illustrated in Fig. 1**e**. In the drug release study at pH 7.4, 97 % of propofol was released after 120 minutes, as shown in Fig. 1**f**.

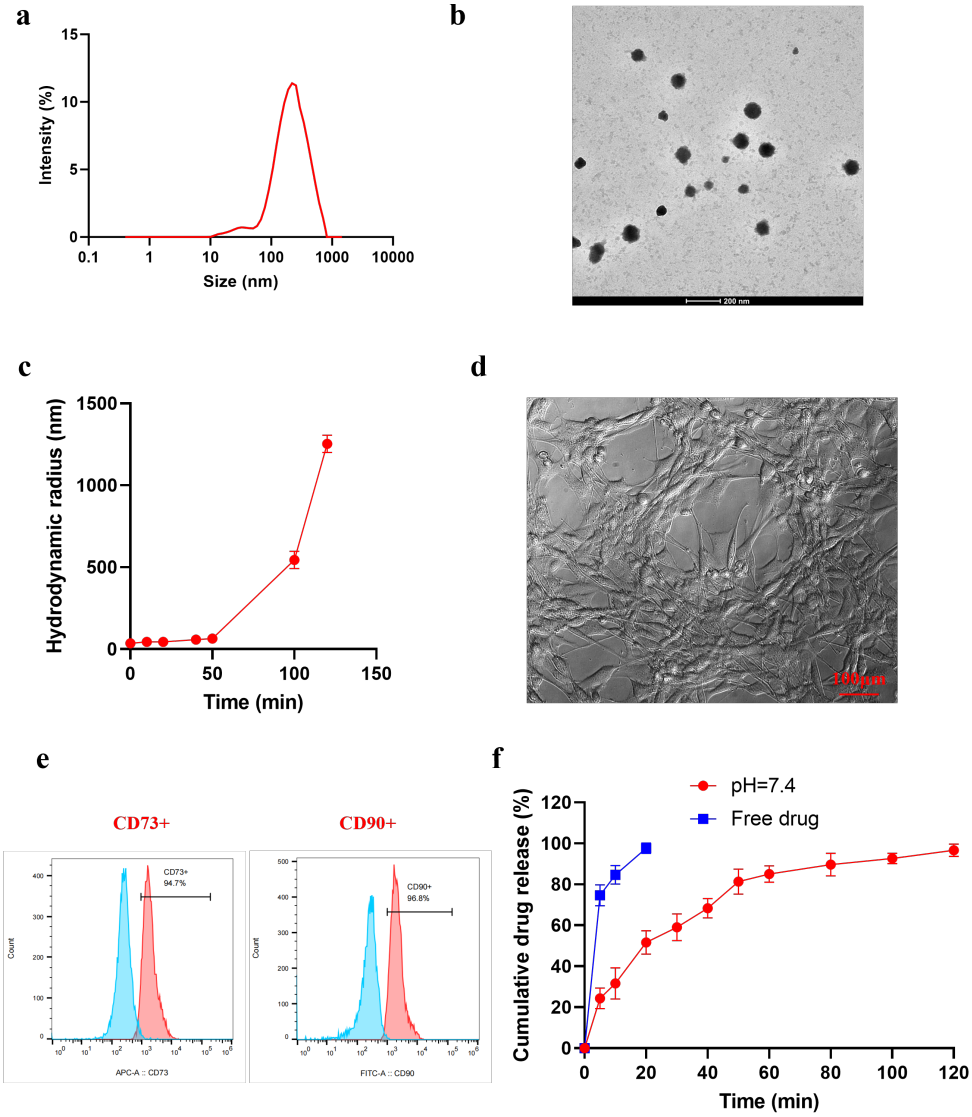


**Fig. 1. Propofol-NPs physicochemical property characterization and bone marrow-derived mesenchymal stem cell (BMSC) identification.** (**a**) Particle size distribution and electron microscopy images. (**b**) Morphology of propofol-NPs. Scale bar, 200 nm. (**c**) Hydrodynamic radius of propofol nanoparticles over time. (**d,e**) BMSCs identification: microscopic features of BMSCs (**d**) and expression levels of surface markers CD73 and CD90 on BMSCs. Scale bar, 100 $\mu$m (**e**). (**f**) Propofol release profile from nanoparticles over 120 minutes. NPs, nanoparticles.

**Table 1. Physicochemical property parameters of nanoparticles.**

| Parameters | Propofol-NPs |
|---|---|
| EE (%) | 65.02 ± 0.54 |
| DL (%) | 32.24 ± 0.39 |
| Particle size (nm) | 126.33 ± 4.59 |
| PDI | 0.11 ± 0.01 |
| Zeta (mV) | –17.23 ± 0.05 |

NPs, nanoparticles; EE, encapsulation efficiency; DL, drug loading; PDI, polymer dispersity index.

*Propofol Promotes Chondrogenesis and Differentiation of BMSCs*

The experimental results from this study demonstrate that the propofol-treated group showed enhanced cartilage formation and fracture healing compared to the control group. As illustrated in Fig. 2**a**,**b**, HE and Masson's staining performed 7 days post-fracture reveal improved cartilage formation and differentiation in both the propofol-treated and propofol-NPs-treated groups. Notably, the propofol-NPs group exhibited superior healing capabilities compared to the propofol group, suggesting that propofol facilitates chondrogenesis and BMSC differentiation, thus accelerating fracture healing. Quantitative analysis shows

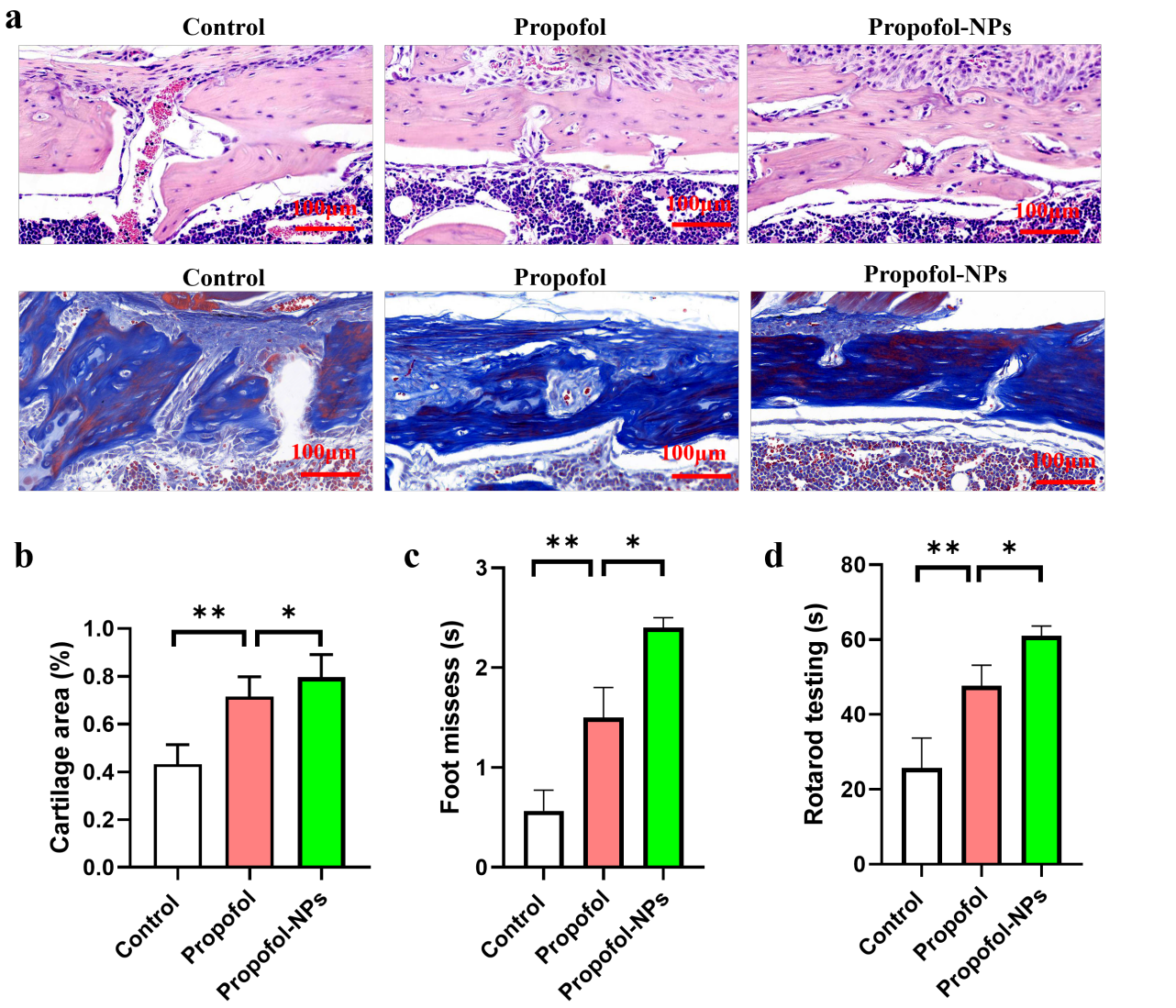


**Fig. 2. Propofol promotes chondrogenesis and chondrocyte differentiation of BMSCs.** (**a**) Hematoxylin and Eosin (HE) and Safranin O staining of fracture tissue 7 days post-injury. Scale bar, 100 $\mu$m. (**b**) Relative proportion of cartilage area in the fracture healing tissue. (**c**) Grid-walking test assessing motor coordination. (**d**) Rotarod test evaluating motor function. *$p < 0.05$, **$p < 0.01$. N = 6.

that the cartilage area in the propofol-treated and propofol-NPs groups was significantly greater than in the control group ($p < 0.01$). Additionally, the cartilage area in the propofol-NPs group was significantly higher than that in the propofol group ($p < 0.05$), indicating a more pronounced effect with nanoparticle administration. Fig. 2**c**,**d** displays the results of the rotating rod and grid walking tests, used to assess functional recovery in fracture mouse models. The data confirm significant improvements in motor recovery following propofol nanoparticle intervention ($p < 0.05$), further supporting the role of propofol in promoting cartilage formation and facilitating fracture healing.

*Propofol Enhances the Ability of BMSCs to Differentiate into Chondrocytes*

Fig. 3**a**,**b** showed that the cell migration capabilities of the control group, propofol group, and propofol-NPs group were assessed using a scratch assay. The results demonstrate that the migration rate in the propofol-treated group was significantly higher than in the control group ($p < 0.01$), with the highest migration rate observed in the propofol-NPs group ($p < 0.05$). This suggests that propofol enhances the migratory ability of BMSCs, contributing to wound healing and cartilage formation. Fig. 3**c** illustrates a significant increase in BMSC activity following intervention with propofol nanoparticles. Furthermore, Fig. 3**d**–**f** illustrated that the migration capability of BMSCs in the propofol group was notably higher than in the control group ($p < 0.01$). This indicates that propofol enhances

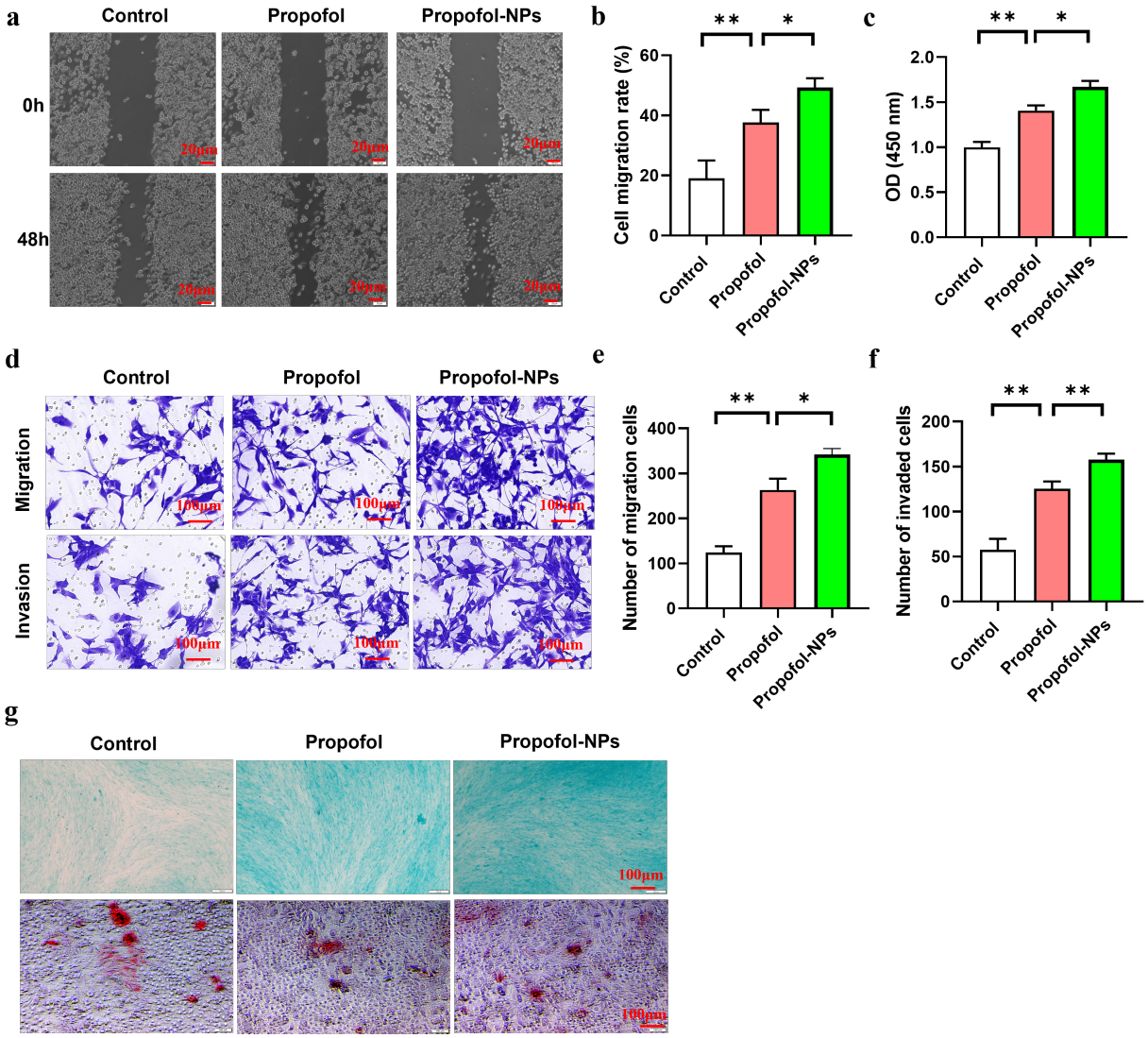


**Fig. 3. Propofol promotes the differentiation of BMSCs into chondrocytes.** (**a**,**b**) Cell scratch assay demonstrating the migration ability of control and propofol-treated groups. Scale bar, 20 $\mu$m. (**c**) Cell viability after propofol-NPs treatment. (**d–f**) Migration ability of control and propofol-treated groups. (**g**) Alcian blue staining showing chondrocytes and alizarin red staining showing osteoblasts. Scale bar, 100 $\mu$m. *$p < 0.05$, **$p < 0.01$. N = 6.

both the migration and invasion potential of BMSCs. As depicted in Fig. 3**g**, Alcian Blue staining results, obtained after 14 days of BMSC culture in a chondrogenic differentiation medium, show a higher staining intensity in the propofol-treated group compared to the control group. The propofol-NPs group exhibited significantly stronger staining than the propofol group, indicating a greater promotion of BMSC differentiation into chondrocytes. However, no significant differences were observed in BMSC differentiation into osteoblasts, suggesting that propofol specifically promotes chondrogenic differentiation of BMSCs.

### *Propofol Enhances the Expression of Differentiation-Related Proteins in BMSCs*

Fig. 4**a**,**b** revealed the impact of propofol on the expression of key proteins in BMSCs 14 days post-differentiation. The expression levels of BMP2, aggrecan, Col2a1, and Alk2 were significantly elevated in the propofol-treated group compared to the control group ($p < 0.05$). Additionally, the propofol-NPs treatment group exhibited markedly higher protein levels of BMP2, aggrecan, Col2a1, and Alk2 compared to the propofol group ($p < 0.05$). These findings suggest that propofol enhances BMSC differentiation into chondrocytes. Furthermore, the phosphorylation of $\beta$-catenin in the Wnt signaling pathway was significantly increased in the propofol-NPs group ($p < 0.001$) (Fig. 4**c**,**d**), indicating a potential mechanism underlying this effect.

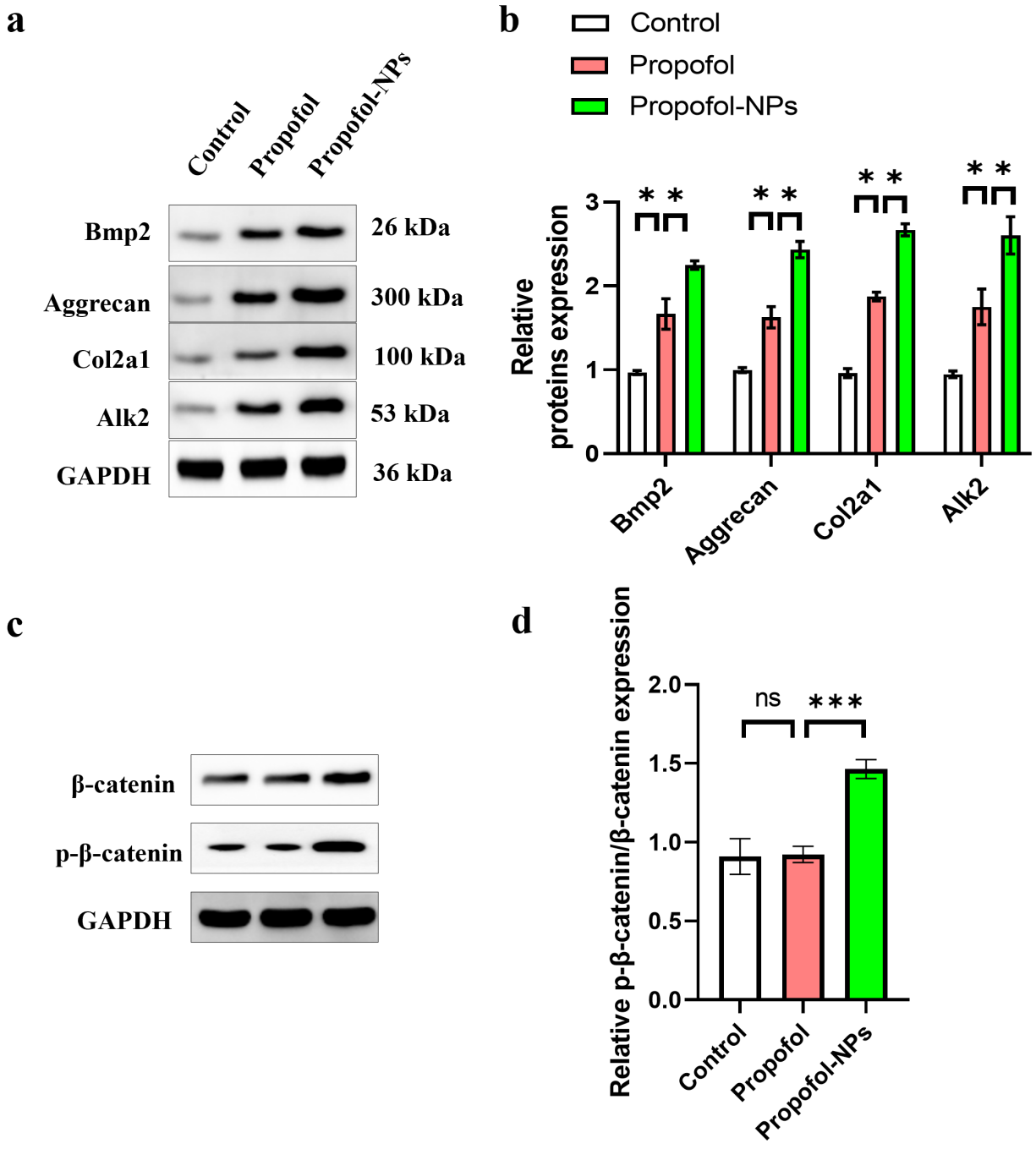


**Fig. 4. Propofol promotes the expression of differentiation-related proteins in BMSCs.** (**a**,**b**) The levels of bone morphogenetic protein 2 (BMP2), aggrecan, Collagen Type II Alpha 1 Chain (Col2a1), and activin receptor-like kinases (Alk)2 in differentiated BMSCs. (**c**,**d**) Protein expression levels of $\beta$-catenin and phosphorylated $\beta$-catenin (p-$\beta$-catenin). Ns, no statistical significance; **$p < 0.01$, ***$p < 0.001$. N = 6.

*Propofol Promotes the Expression of OSX and COL1 Proteins*

As illustrated in Fig. 5**a–d**, the effects of propofol on the expression of OSX and COL1 in BMSCs were evaluated after 14 days of differentiation. The results demonstrate significantly higher levels of OSX and COL1 proteins after propofol and propofol-NPs treatment ($p < 0.01$). Moreover, the propofol-NPs group exhibited a more pronounced therapeutic effect than the propofol group ($p < 0.05$) (Fig. 5**a–c**), indicating that propofol promotes BMSC differentiation into osteoblasts. Collectively, these findings suggest that propofol facilitates fracture healing by enhancing the expression of OSX and COL1, thereby promoting intracondral bone formation during the healing process.

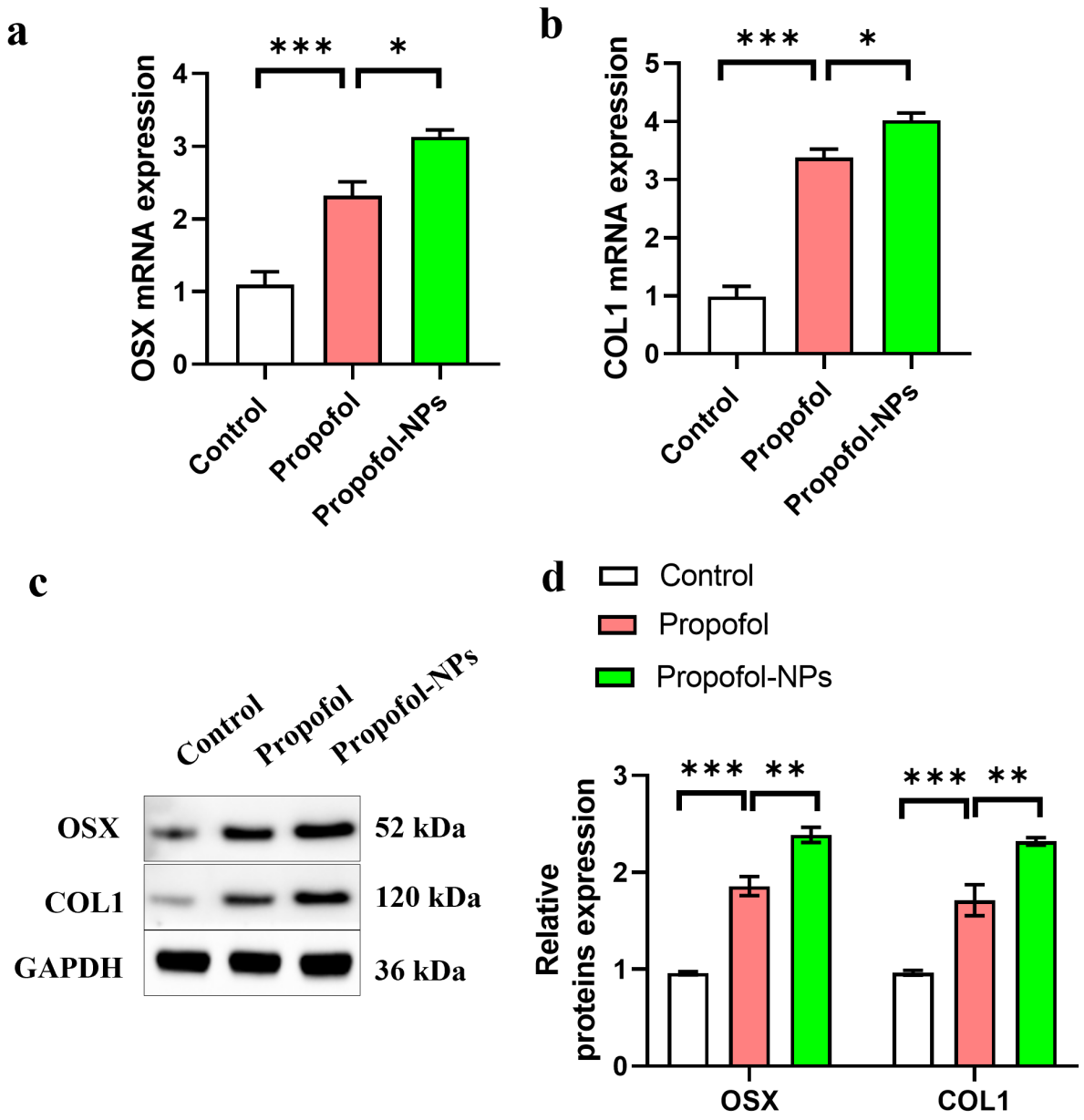


**Fig. 5. Propofol promotes the expression of osterix (OSX) and collagen I (COL1) proteins.** (**a**) The mRNA level of OSX in BMSCs. (**b**) The mRNA level of COL1 in BMSCs. (**c,d**) The levels of OSX and COL1 proteins in differentiated BMSCs. *$p < 0.05$, **$p < 0.01$, ***$p < 0.001$. N = 6.

## Discussion

Cartilage plays a vital role in fracture healing by serving as a temporary scaffold for new bone tissue (Sollender *et al*., 2019). Fracture repair primarily occurs through endochondral ossification (Hu *et al*., 2017), a process that involves the formation of cartilage and its subsequent transition into bone (Kodama *et al*., 2022). In our study, using a mouse fracture model, treatment with propofol nanoparticles resulted in enhanced cartilage formation and restoration of motor function in the mice. Additionally, previous research has identified OSX and COL1 as markers of endochondral ossification (Yan *et al*., 2023). A positive feedback loop exists between chondrogenesis and intrachondral ossification during fracture healing, while endochondral ossification is inversely related to the overall recovery process. Our findings align with this, as the expression levels of OSX and COL1 increased after propofol nanoparticle treatment in fractured mice, indicating that propofol may promote fracture healing by stimulating intrachondral ossification.

BMSCs possess the ability to differentiate into various cell types, including osteoblasts, adipocytes, chondrocytes, muscle cells, and fibroblasts (Bahney *et al*., 2019).

Chondrodifferentiation is critical for cartilage regeneration, as differentiated chondrocytes facilitate stable cartilage formation (Hollander *et al*., 2010). To further explore the role of propofol nanoparticles in cartilage formation, our study demonstrated that propofol nanoparticles enhanced the chondrogenic differentiation of BMSCs, as evidenced by distinct staining patterns following treatment. Moreover, this study assessed the expression of BMP2, aggrecan, and Col2a1, all of which are closely linked to cartilage formation (Yan *et al*., 2023). BMP2 is integral to the regulation of chondrocyte proliferation and maturation during intrachondral bone development (Shu *et al*., 2011). BMP2 has been shown to induce cartilage formation and is beneficial for cartilage regeneration, particularly in the context of BMSC differentiation into chondrocytes (Kwon *et al*., 2013). Aggrecan and Col2a1 are also highly expressed during cartilage differentiation (Lu *et al*., 2020). In line with our findings, propofol nanoparticles not only upregulated BMP2 expression but also increased the levels of aggrecan and Col2a1, further supporting their role in promoting cartilage differentiation.

These results suggest that propofol may activate signaling pathways, including BMP2, to enhance cartilage formation and accelerate fracture healing. Numerous studies have also highlighted the critical role of the Wnt/$\beta$-catenin signaling pathway in fracture healing and mesenchymal stem cell differentiation (Liu *et al*., 2020a; Pan *et al*., 2021). The observed promotion of $\beta$-catenin phosphorylation by propofol nanoparticles indicates that the BMP2/Wnt/$\beta$-catenin signaling axis may be a key mechanism through which propofol nanoparticles facilitate cartilage formation and fracture repair.

Propofol is a commonly used anesthetic and analgesic, with its safety and pharmacokinetic properties well-documented (Hausburg *et al*., 2020; Zhang *et al*., 2021). As a result, its potential clinical application in fracture healing appears promising. However, further clinical studies are required to confirm propofol's efficacy and safety in this context. Future research could focus on several key areas: first, a deeper investigation into the molecular mechanisms of propofol's effects on chondrocyte differentiation and cartilage matrix calcification, providing more detailed insights into its role in promoting fracture healing; second, more extensive animal studies and clinical trials to establish both the safety and effectiveness of propofol in enhancing fracture repair; and third, the integration of biomaterials and tissue engineering approaches to develop novel application strategies, such as drug-loaded scaffolds or bioprinting techniques for fracture healing.

This study has several limitations. First, the evaluation of chondrogenic differentiation in BMSCs was performed using a relatively basic method, alcian blue staining. Future studies should employ additional markers and more sophisticated techniques to further validate BMSC chondrogenic differentiation. Second, while evidence of chondrogenic differentiation was observed, it was only assessed at a single time point. Subsequent research should track BMSC differentiation and protein expression over various time intervals to better understand the process. Third, this study did not investigate alternative mechanisms involved in propofol's effects on fracture healing. Future molecular studies are necessary to address this gap and provide a more comprehensive understanding of propofol's mechanisms of action.

## Conclusions

Our findings indicate that propofol and propofol-NPs may facilitate fracture healing by accelerating cartilage formation, offering a novel perspective on the potential use of propofol in this context. Nevertheless, the precise mechanisms underlying propofol's effects on fracture healing, as well as its clinical applicability, warrant further investigation. This study serves as a reference point and provides valuable insights for future research and clinical applications of propofol in promoting fracture repair.

## List of Abbreviations

Alk, activin receptor-like kinases; ALP, alkaline phosphatase; BMP, bone morphogenetic protein; BMSCs, bone marrow-derived mesenchymal stem cells; COL1, collagen I; Col2a1, Collagen Type II Alpha 1 Chain; DL, drug loading; DLS, dynamic light scattering; EDTA, ethylenediaminetetraacetic acid; FGF, fibroblast growth factor; HE, Hematoxylin and Eosin; HRP, horseradish peroxidase; NPs, nanoparticles; OSX, osterix; PDI, polymer dispersity index; PVP, polyvinylpyrrolidone; SD, standard deviation; Wnt, wingless-related integration site; EE, encapsulation efficiency; PBS, phosphate-buffered saline; CCK-8, Cell Counting Kit-8; p-$\beta$-catenin, phosphorylated $\beta$-catenin; FBS, fetal bovine serum.

## Availability of Data and Materials

Data to support the findings of this study are available on reasonable request from the corresponding author.

## Author Contributions

BYZ and ZW designed the study. SJY and HW collected and analyzed the data. HW and BYZ participated in drafting the manuscript. All authors conducted the study and contributed to critical revision of the manuscript for important intellectual content. All authors gave final approval of the version to be published. All authors participated fully in the work, took public responsibility for appropriate portions of the content, and agreed to be accountable for all aspects of the work in ensuring that questions related to the accuracy or completeness of any part of the work were appropriately investigated and resolved.

## Ethics Approval and Consent to Participate

This study has been approved by the Ethics Committee of The Second Affiliated Hospital of Shandong First Medical University, approval No. 2022-079.

## Acknowledgments

Not applicable.

## Funding

This research received no external funding.

## Conflict of Interest

The authors declare no conflict of interest.

## References

Bahney CS, Zondervan RL, Allison P, Theologis A, Ashley JW, Ahn J, Miclau T, Marcucio RS, Hankenson KD (2019) Cellular biology of fracture healing. Journal of Orthopaedic Research: Official Publication of the Orthopaedic Research Society 37: 35-50. DOI: 10.1002/jor.24170.

Chen H, He L, Li D, Jin F, Ai Y (2021) Propofol-loaded nanomicelle with improved anesthetic, pharmacokinetic, hemocompatibility, safety, and permeation profiles. Arabian Journal of Chemistry 14: 103093. DOI: 10.1016/j.arabjc.2021.103093.

Cheng Z, Li A, Tu CL, Maria CS, Szeto N, Herberger A, Chen TH, Song F, Wang J, Liu X, Shoback DM, Chang W (2020) Calcium-Sensing Receptors in Chondrocytes and Osteoblasts Are Required for Callus Maturation and Fracture Healing in Mice. Journal of Bone and Mineral Research: the Official Journal of the American Society for Bone and Mineral Research 35: 143-154. DOI: 10.1002/jbmr.3864.

Chilbule SK, Rajagopal K, Walter N, Dutt V, Madhuri V (2021) Role of WNT Agonists, BMP and VEGF Antagonists in Rescuing Osteoarthritic Knee Cartilage in a Rat Model. Indian Journal of Orthopaedics 56: 24-33. DOI: 10.1007/s43465-021-00434-1.

Clark D, Brazina S, Yang F, Hu D, Hsieh CL, Niemi EC, Miclau T, Nakamura MC, Marcucio R (2020) Age-related changes to macrophages are detrimental to fracture healing in mice. Aging Cell 19: e13112. DOI: 10.1111/acel.13112.

Deng Z, Gao X, Sun X, Cui Y, Amra S, Huard J (2020) Gender differences in tibial fractures healing in normal and muscular dystrophic mice. American Journal of Translational Research 12: 2640-2651.

Ghiasi MS, Chen JE, Rodriguez EK, Vaziri A, Nazarian A (2019) Computational modeling of human bone fracture healing affected by different conditions of initial healing stage. BMC Musculoskeletal Disorders 20: 562. DOI: 10.1186/s12891-019-2854-z.

Hausburg MA, Banton KL, Roman PE, Salgado F, Baek P, Waxman MJ, Tanner A 2nd, Yoder J, Bar-Or D (2020) Effects of propofol on ischemia-reperfusion and traumatic brain injury. Journal of Critical Care 56: 281-287. DOI: 10.1016/j.jcrc.2019.12.021.

Hollander AP, Dickinson SC, Kafienah W (2010) Stem cells and cartilage development: complexities of a simple tissue. Stem Cells 28: 1992-1996. DOI: 10.1002/stem.534.

Hu DP, Ferro F, Yang F, Taylor AJ, Chang W, Miclau T, Marcucio RS, Bahney CS (2017) Cartilage to bone transformation during fracture healing is coordinated by the invading vasculature and induction of the core pluripotency genes. Development 144: 221-234. DOI: 10.1242/dev.130807.

Kim JH, Kim M, Hong S, Kim EY, Lee H, Jung HS, Sohn Y (2021) Albiflorin Promotes Osteoblast Differentiation and Healing of Rat Femoral Fractures Through Enhancing BMP-2/Smad and Wnt/$\beta$-Catenin Signaling. Frontiers in Pharmacology 12: 690113. DOI: 10.3389/fphar.2021.690113.

Kodama J, Wilkinson KJ, Iwamoto M, Otsuru S, Enomoto-Iwamoto M (2022) The role of hypertrophic chondrocytes in regulation of the cartilage-to-bone transition in fracture healing. Bone Reports 17: 101616. DOI: 10.1016/j.bonr.2022.101616.

Kwon SH, Lee TJ, Park J, Hwang JE, Jin M, Jang HK, Hwang NS, Kim BS (2013) Modulation of BMP-2-induced chondrogenic versus osteogenic differentiation of human mesenchymal stem cells by cell-specific extracellular matrices. Tissue Engineering. Part A 19: 49-58. DOI: 10.1089/ten.TEA.2012.0245.

Lee DW, Kwon JY, Kim HK, Lee HJ, Kim ES, Kim HJ, Kim HJ, Lee HB (2018) Propofol attenuates osteoclastogenesis by lowering RANKL/OPG ratio in mouse osteoblasts. International Journal of Medical Sciences 15: 723-729. DOI: 10.7150/ijms.22713.

Liu D, Qin H, Yang J, Yang L, He S, Chen S, Bao Q, Zhao Y, Zong Z (2020a) Different effects of Wnt/$\beta$-catenin activation and PTH activation in adult and aged male mice metaphyseal fracture healing. BMC Musculoskeletal Disorders 21: 110. DOI: 10.1186/s12891-020-3138-3.

Liu M, Alharbi M, Graves D, Yang S (2020b) IFT80 Is Required for Fracture Healing Through Controlling the Regulation of TGF-$\beta$ Signaling in Chondrocyte Differentiation and Function. Journal of Bone and Mineral Research: the Official Journal of the American Society for Bone and Mineral Research 35: 571-582. DOI: 10.1002/jbmr.3902.

Lu Y, Zhou L, Wang L, He S, Ren H, Zhou N, Hu Z (2020) The role of SIRT1 in BMP2-induced chondrogenic differentiation and cartilage maintenance under oxidative stress. Aging 12: 9000-9013. DOI: 10.18632/aging.103161.

Luo J, Wang D, Guo W, Cao H (2020) Anesthesia Effect of Propofol Nanoinjection Combined with Nerve Block. Nanoscience and Nanotechnology Letters 12: 512-

517. DOI: 10.1166/nnl.2020.3130.

Pan FF, Shao J, Shi CJ, Li ZP, Fu WM, Zhang JF (2021) Apigenin promotes osteogenic differentiation of mesenchymal stem cells and accelerates bone fracture healing via activating Wnt/$\beta$-catenin signaling. American Journal of Physiology. Endocrinology and Metabolism 320: E760-E771. DOI: 10.1152/ajpendo.00543.2019.

Peng X, Li C, Yu W, Liu S, Cong Y, Fan G, Qi S (2020) Propofol Attenuates Hypoxia-Induced Inflammation in BV2 Microglia by Inhibiting Oxidative Stress and NF-$\kappa$B/Hif-1$\alpha$ Signaling. BioMed Research International 2020: 8978704. DOI: 10.1155/2020/8978704.

Saul D, Khosla S (2022) Fracture Healing in the Setting of Endocrine Diseases, Aging, and Cellular Senescence. Endocrine Reviews 43: 984-1002. DOI: 10.1210/endrev/bnac008.

Schlickewei CW, Kleinertz H, Thiesen DM, Mader K, Priemel M, Frosch KH, Keller J (2019) Current and Future Concepts for the Treatment of Impaired Fracture Healing. International Journal of Molecular Sciences 20: 5805. DOI: 10.3390/ijms20225805.

Shu B, Zhang M, Xie R, Wang M, Jin H, Hou W, Tang D, Harris SE, Mishina Y, O'Keefe RJ, Hilton MJ, Wang Y, Chen D (2011) BMP2, but not BMP4, is crucial for chondrocyte proliferation and maturation during endochondral bone development. Journal of Cell Science 124: 3428-3440. DOI: 10.1242/jcs.083659.

Sivaraj KK, Majev PG, Jeong HW, Dharmalingam B, Zeuschner D, Schröder S, Bixel MG, Timmen M, Stange R, Adams RH (2022) Mesenchymal stromal cell-derived septoclasts resorb cartilage during developmental ossification and fracture healing. Nature Communications 13: 571. DOI: 10.1038/s41467-022-28142-w.

Sollender GE, White TW, Pieracci FM (2019) Fracture of the Costal Cartilage: Presentation, Diagnosis, and Management. The Annals of Thoracic Surgery 107: e267-e268. DOI: 10.1016/j.athoracsur.2018.08.076.

Xu Y, Pan S, Jiang W, Xue F, Zhu X (2020) Effects of propofol on the development of cancer in humans. Cell Proliferation 53: e12867. DOI: 10.1111/cpr.12867.

Yan W, Shen M, Sun K, Li S, Miao J, Wang J, Xu J, Wen P, Zhang Q (2023) Norisoboldine, a Natural Isoquinoline Alkaloid, Inhibits Diaphyseal Fracture Healing in Mice by Alleviating Cartilage Formation. Biomedicines 11: 2031. DOI: 10.3390/biomedicines11072031.

Zhang C, Feinberg D, Alharbi M, Ding Z, Lu C, O'Connor JP, Graves DT (2019) Chondrocytes Promote Vascularization in Fracture Healing Through a FOXO1-Dependent Mechanism. Journal of Bone and Mineral Research: the Official Journal of the American Society for Bone and Mineral Research 34: 547-556. DOI: 10.1002/jbmr.3610.

Zhang R, Lee P, Lui VCH, Chen Y, Liu X, Lok CN, To M, Yeung KWK, Wong KKY (2015) Silver nanoparticles promote osteogenesis of mesenchymal stem cells and improve bone fracture healing in osteogenesis mechanism mouse model. Nanomedicine: Nanotechnology, Biology, and Medicine 11: 1949-1959. DOI: 10.1016/j.nano.2015.07.016.

Zhang X, Li S, Liu J (2021) Efficacy and safety of remimazolam besylate versus propofol during hysteroscopy: single-centre randomized controlled trial. BMC Anesthesiology 21: 156. DOI: 10.1186/s12871-021-01373-y.

Zhang Y, Zuo T, McVicar A, Yang HL, Li YP, Chen W (2022) Runx1 is a key regulator of articular cartilage homeostasis by orchestrating YAP, TGF$\beta$, and Wnt signaling in articular cartilage formation and osteoarthritis. Bone Research 10: 63. DOI: 10.1038/s41413-022-00231-y.

Zhou W, Lin Z, Xiong Y, Xue H, Song W, Yu T, Chen L, Hu Y, Panayi AC, Sun Y, Cao F, Liu G, Hu L, Yan C, Xie X, Qiu W, Mi B, Liu G (2021) Dual-Targeted Nanoplatform Regulating the Bone Immune Microenvironment Enhances Fracture Healing. ACS Applied Materials & Interfaces 13: 56944-56960. DOI: 10.1021/acsami.1c17420.

Zhu S, Bennett S, Kuek V, Xiang C, Xu H, Rosen V, Xu J (2020) Endothelial cells produce angiocrine factors to regulate bone and cartilage via versatile mechanisms. Theranostics 10: 5957-5965. DOI: 10.7150/thno.45422.

**Editor's note**: The Scientific Editor responsible for this paper was Chris Evans.